CHEMISTRY
A EUROPEAN JOURNAL

DOI: 10.1002/chem.200801127

# A Comparison of $N_2$ Cleavage in Schrock's $Mo[N_3N]$ and Laplaza–Cummins' $Mo[N(R)Ar]_3$ Systems

**Gemma Christian,[a] Robert Stranger,*[a] and Brian F. Yates[b]**

**Abstract:** The four-coordinate $Mo[N_3N]$ complex, $[N_3N] = [\{RNCH_2CH_2\}_3N]$, R = 3,5-(2,4,6-$i$Pr$_3$C$_6$H$_2$)$_2$C$_6$H$_3$ (HIPT), which is capable of converting $N_2$ to ammonia catalytically, reacts with $N_2$ in a similar manner to $Mo[N(R)Ar]_3$ (R = $t$Bu, Ar = 3,5-$C_6H_3Me_2$) to form a dinitrogen-bridged dimer intermediate, but unlike its three-coordinate counterpart, $N_2$ cleavage is not observed. To rationalise these differences, the reaction of $N_2$ with the model $Mo[NH_2]_3[NH_3]$ and full ligand $Mo[N_3N]$ systems was explored using density functional theory and compared with the results of an earlier study involving the model three-coordinate $Mo[NH_2]_3$ system. Although the overall reaction is exothermic, the final N–N cleavage step is calculated to be endothermic by 75 kJ mol$^{-1}$ for the model system when the Mo–amine cap bond length is fixed to mimic the constraints of the ligand straps, but exothermic by 14 kJ mol$^{-1}$ for the full ligand system. In the latter case, the slightly exothermic cleavage step can be attributed to the destabilization of the $N_2$ bridged dimer relative to the nitride product owing to the steric effects of the bulky R groups. The activation barrier for N–N cleavage is estimated at 151 kJ mol$^{-1}$ for the model system, more than twice the calculated value for $Mo[NH_2]_3$, and even greater, 213 kJ mol$^{-1}$, for the full ligand $[N_3N]Mo$ system. A bonding analysis shows that although the binding of the amine cap helps to stabilize the intermediate dimer, at the same time it destabilizes the metal d-orbitals involved in backbonding to the $\pi^*$ orbitals on $N_2$. As a result, backdonation is less efficient and N–N activation reduced compared to the three-coordinate system. Thus, the increased stability of the intermediate dimer on binding of the amine cap combined with the reduced level of N–N activation and higher kinetic barrier, explain why N–N cleavage has not been observed experimentally for the four-coordinate $Mo[N_3N]$ system.

**Keywords:** density functional calculations · dimerization · molybdenum · nitrogen fixation · structure–activity relationships

## Introduction

The high temperatures (400–550 °C) and pressures (100–300 atm) necessary to drive the Haber–Bosch process, the main commercial route used to produce ammonia from $N_2$, have prompted significant efforts to develop transition metal systems that are capable of activating and cleaving dinitrogen under mild conditions.[1–6] On this note, one of the most interesting recent discoveries in the field of $N_2$ activation is the catalytic conversion of $N_2$ to ammonia by the four-coordinate $Mo[N_3N]$ complex of Schrock and co-workers,[7,8] in which $[N_3N] = [\{RNCH_2CH_2\}_3N]$, R = 3,5-(2,4,6-$i$Pr$_3$C$_6$H$_2$)$_2$C$_6$H$_3$ (HIPT). With an appropriate proton source and reductant, the system can be cycled at least four times.[7,9]

The chemistry of $M[N_3N]$ complexes is diverse,[10] with $M[N_3N]$ or $[N_3N]M–L$ complexes synthesised for most first row and many second and third row transition metals.[11,12,13,14] The $N_3N$ ligand binds to metals in a tetradentate manner, creating a ligand cage with an amine cap,[10] as shown in Figure 1. With the exception of the cap, the $N_3N$ ligand system is similar to Laplaza and Cummins $M[N(R)Ar]_3$ (R = $t$Bu, Ar = 3,5-$C_6H_3Me_2$) system,[15–17] in that it has three amide donors arranged in a trigonal plane around the metal centre, a similar orientation of the R groups, and the same overall charge on the metal complex. Analogous to $M[N(R)Ar]_3$, the metal based σ ($d_{z^2}$) and π ($d_{xz}$, $d_{yz}$) orbitals are available for binding to additional li-

[a] Dr. G. Christian, Prof. R. Stranger
Department of Chemistry, Faculty of Science
Australian National University
Canberra, ACT 0200 (Australia)
Fax: (+61) 2-6125-0760
E-mail: rob.stranger@anu.edu.au

[b] Prof. B. F. Yates
School of Chemistry
University of Tasmania
Private Bag 75, Hobart, TAS 7001 (Australia)

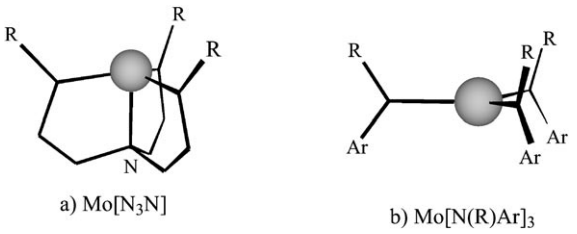


Figure 1. Coordination geometries for $Mo[N_3N]$ ($N_3N = [(RNCH_2CH_2)_3N]^{3-}$) and $Mo[N(R)Ar]_3$ in which R is a bulky group.

gands, and the R groups restrict access so that only small molecules can reach the metal centre through the sterically protected pocket trans to the nitrogen cap.

Both $Mo[N_3N]$ and $Mo[N(R)Ar]_3$ react with $N_2$ to form the encounter complex $N_2$–MoL (L = $N_3N$ or N(R)Ar). If the R groups are not too large, binding of a second MoL complex occurs to give the LMo–$N_2$–MoL dimer intermediate with $N_2$ bridging end-on between the metal centres. Both $N_2$–$\{Mo[N_3N]\}_2$ and $N_2$–$\{Mo[N(R)Ar]_3\}_2$ dimers have been successfully characterised by X-ray crystallography, with reported N–N bond distances of 1.20 and 1.21 Å, respectively.[18,19] In the latter case, the N–N bond is completely severed to form two equivalents of N–$Mo[N(R)Ar]_3$ under very-mild conditions,[6,15,17] whereas no N–N bond cleavage has been observed for $N_2$–$\{Mo[N_3N]\}_2$.[18,20,21] Because of the unreactivity of the $N_2$–$\{Mo[N_3N]\}_2$ dimer, Schrock et al. used large R groups, such as HIPT to prevent its formation, thus limiting the reaction to the formation of $N_2$–$Mo[N_3N]$.[20–22] The $[N_3N]Mo$–$N_2$ encounter complex, which is the starting point for the catalytic cycle, has been isolated[12,23] and structurally characterised,[23] unlike $[Ar(R)N]_3Mo$–$N_2$ which has not been directly observed. The stability of $[N_3N]Mo$–$N_2$ over its three-coordinate counterpart has been attributed to the interaction of the amine cap which destabilizes the $d_{z^2}$ orbital sufficiently to favour the doublet spin state over the spin quartet, the former being the optimal spin state for binding $N_2$.

As part of a broader DFT investigation of the $N_2$ cleavage reaction involving the $Mo[N(R)Ar]_3$ system, Cui et al[22] carried out a brief computational study of $N_2$ cleavage by $Mo[N_3N]$ by using a model system which incorporated the ligand straps but replaced the bulky R groups with H. The N–N cleavage step was calculated to be endothermic by 42 kJ mol$^{-1}$, in contrast with the $Mo[N(R)Ar]_3$ system in which the same step was calculated to be 113 kJ mol$^{-1}$ exothermic. Based on these results, they concluded that the Mo–$N_{ax}$ σ interaction competes with the Mo–$N_2$ σ interaction in the $Mo[N_3N]$ system, leading to a weakening of the Mo–$N_2$ bond throughout the reaction, making $N_2$ cleavage kinetically and thermodynamically unfavourable. Extended Hückel calculations have also been carried out to rationalise the paramagnetism of $N_2$–$\{Mo[N_3N]\}_2$.[20]

There have been a number of computational studies of the catalytic conversion of $N_2$ to $NH_3$ by $Mo[N_3N]$.[24–28] but in general these focus on $N_2$ activation at a single metal centre rather than N–N cleavage through a bimetallic mechanism. Each step in the catalytic reaction has been studied in detail using DFT on the model $Mo[N_3N]$ system with R = H,[24,25] $C_5H_5$,[26] or 3,5-$(C_6H_5)_2C_6H_3$.[27] Calculations have also been carried out using the smallest of the full ligands with R = 3,5-$(2,4,6\text{-}Me_3C_6H_2)_2C_6H_3$.[27,28] The use of the full ligand has been shown to be important in calculating accurate energies.[27]

Although there have been suggestions about the role of the ligand cap in the $N_2$ cleavage reaction, its effect on the bonding and activation of $N_2$ has not been examined in detail. The present study therefore explores the electronic differences between the $Mo[N_3N]$ and $Mo[N(R)Ar]_3$ systems, with a focus on understanding why $Mo[N_3N]$ does not cleave the N–N bond directly, in contrast to its three-coordinate counterpart. To accomplish this, the reaction profile for both the experimental $Mo[N_3N]$ (R = *t*Bu) system and the model $Mo[NH_2]_3[NH_3]$ system in which the ligand straps and R groups have been replaced by hydrogen, are examined in detail. Although $NH_2$ and $NH_3$ are not accurate models of the larger ligands, the smaller model system allows us to study the effect of the amine cap on the bonding in the absence of steric strain, and without the restrictions imposed by the ligand straps. Following this, a bonding analysis is undertaken for the model system to determine the effect of the amine cap on $N_2$ activation and cleavage. As, with the exception of the amine cap, the coordination environment in $Mo[N_3N]$ is similar to $Mo[N(R)Ar]_3$, and the ligand charge and metal are the same, it is possible to directly compare these two systems and thus investigate the influence of the ligand cap on the reaction energetics.

## Computational Details

The calculations carried out in this work were performed by using the Amsterdam density functional (ADF)[29–31] program (version 2002.03 and 2006.01) running on either Linux-based PCs or the Australian National University Supercomputing Facility. All calculations used the local density approximation (LDA) to the exchange potential, the correlation potential of Vosko, Wilk and Nusair (VWN),[32] the Becke[33] and Perdew[34] corrections for non-local exchange and correlation, and the numerical integration scheme of te Velde and co-workers.[35] Geometry optimisations were performed by using the gradient algorithm of Versluis and Ziegler.[36] All electron, triple-ζ Slater type orbital basis sets with a single polarization function (TZP) were used for all atoms. Relativistic effects were incorporated using the zero order relativistic approximation (ZORA).[37–39] Frequencies were computed by numerical differentiation of energy gradients in slightly displaced geometries.[40,41] All calculations were carried out in a spin-unrestricted manner and frequency calculations for the model system were used to confirm that the optimized structures of lowest energy were true minima. Free energies were evaluated for the model system. The convergence criteria for geometry optimisations were

  

$10^{-3}$ Hartrees for energy and $10^{-2}$ Hartrees/angstrom for gradient. SCF convergence was set at $10^{-6}$. The integration parameter, accint, was set to 4.0 for geometry optimisations and to 6.0 for frequency calculations. Bond energies were analysed using the fragment-based bond decomposition scheme available in ADF.[42–44]

For calculations on the experimental M[$N_3$N] system with R = *t*Bu, the QM/MM[45] method implemented in ADF was used. For these calculations the electronically important regions of the molecule, which include the metal centre, $N_2$ and the N donor atoms from the amide ligands, were treated with DFT, whereas the R groups were treated with molecular mechanics using the Sybyl[46] force field. The ligand straps were included in the DFT region, as preliminary calculations with the straps in the MM region were problematic. UFF Van der Waals parameters[47] were used for Mo whereas all other parameters involving the metal atoms were set to zero. The bonds that cross the QM/MM partition, known as link bonds, were "capped" by H for the QM region. The ratio of the link bond to the length of the capping bond was kept constant throughout the calculations corresponding to the link bond parameters being fixed at values of $\alpha_{(N\text{-}CR)} = 1.47735$. The link bond parameter was calculated using the N-$C_R$ bond length from full QM calculations on Mo[$N_3$N] with R = H and *t*Bu. All QM/MM calculations were undertaken in $C_1$ symmetry.

## Results and Discussion

**Structures and energies**: DFT calculations on Schrock's Mo[$N_3$N] system were undertaken on the model complex, Mo[$NH_2$]$_3$[$NH_3$], in which the R groups and ligand straps were replaced by $NH_2$ and a $NH_3$ cap, and also the full ligand system, Mo[$N_3$N] (R = *t*Bu), using QM/MM methods. In the latter calculations, the R groups form the MM region whereas the ligand backbone and cap are included in the QM region, therefore extending on the calculations carried out by Cui et al[22] which excluded the ligand R group. Apart from the obvious computational efficiencies, the advantage of using the model system is that it is more straightforward to study the effect of the amine cap on the energy, structure and bonding in the system. In particular, a symmetry based bonding analysis would not be possible for the Mo[$N_3$N] complex as the ligand straps lower the molecular point group to $C_3$ symmetry which currently cannot be accommodated in the ADF package, thereby necessitating the calculations to be run in $C_1$ symmetry. Furthermore, the Mo[$NH_2$]$_3$[$NH_3$] model makes it possible to directly compare with our previous work on Mo[$NH_2$]$_3$ used to model the three-coordinate Laplaza-Cummins system.[48]

Experimentally, Cl–Mo[$N_3$N] is used as the starting material rather than Mo[$N_3$N] which cannot be isolated. However, in order to make a straightforward comparison with the three-coordinate Mo[N(R)Ar]$_3$ system, Mo[$N_3$N] was used to calculate the overall reaction profile. Geometry optimisations on both the model and full ligand systems were carried out for the reactants, Mo[$NH_2$]$_3$[$NH_3$] and Mo[$N_3$N], $N_2$ encounter complexes, $N_2$–Mo[$NH_2$]$_3$[$NH_3$] and $N_2$–Mo[$N_3$N], intermediate dimers, [$NH_3$][$NH_2$]$_3$Mo–$N_2$–Mo[$NH_2$]$_3$[$NH_3$] and [$N_3$N]Mo–$N_2$–Mo[$N_3$N], and nitride products, N–Mo[$NH_2$]$_3$[$NH_3$] and N–Mo[$N_3$N]. For Mo[$NH_2$]$_3$[$NH_3$], the structures were initially constrained to $C_{3v}$ symmetry to reflect the geometry of the experimental Mo[$N_3$N] complex. The optimised model and full ligand structures are shown in Figure 2 and selected bond lengths are summarised in Table 1.

For the model system, the optimized Mo–$N_{ax}$ bond lengths associated with the amine cap of 2.675 and 2.877 Å for the reactant and product, respectively, are considerably longer than the Mo–$N_{ax}$ values reported in experiment for N–Mo[$N_3$N],[12,20,21,49] owing to the absence of the ligand

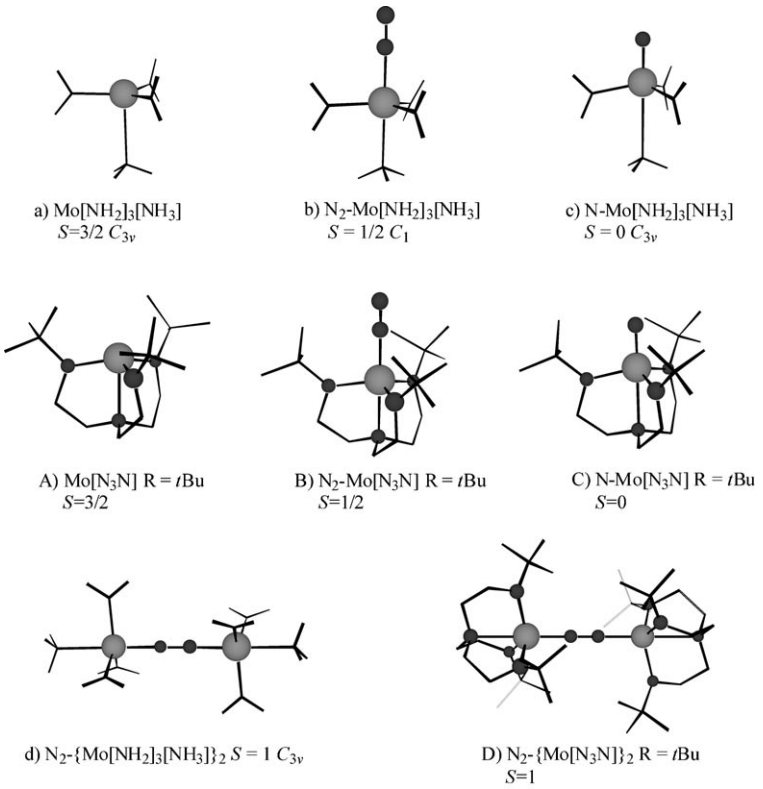


Figure 2. Minimum structures for reactant, encounter complex, product and intermediate dimer for model Mo[$NH_2$]$_3$[$NH_3$] (a–d) and full-ligand Mo[$N_3$N] systems (A–D).

  

Table 1. Selected bond lengths [Å] from the optimised structures of reactant, encounter complex, intermediate dimer and product for the model $Mo[NH_2]_3[NH_3]$ and full-ligand $Mo[N_3N]$ systems. Experimental values are included if available (italics).

| Complex | Spin | Geometry | Mo–$N_{ax}$ | Mo–$N_{am}$ | Mo–N | N–N |
|---|---|---|---|---|---|---|
| $Mo[NH_2]_3[NH_3]$ | 3/2 | $C_{3v}$ | 2.675 | 1.992 | | |
| $Mo[N_3N]$ | 3/2 | $C_1$ | 2.380 | 2.006 | | |
| $N_2$–$Mo[NH_2]_3[NH_3]$ | 1/2 | $C_1$ | 2.289 | 1.993 | 1.968 | 1.146 |
| $N_2$–$Mo[N_3N]$ | 1/2 | $C_1$ | 2.211 | 2.032 | 1.989 | 1.148 |
| | | *exptl* | *2.197* | *1.993* | *1.993* | *1.084*[21] |
| $N_2$–$\{Mo[NH_2]_3[NH_3]\}_2$ | 0 | $C_{3v}$ | 2.305, 2.308 | 1.994 | 1.901 | 1.194 |
| | | $C_1$ | 2.322, 2.325 | 1.996 | 1.897 | 1.195 |
| | 1 | $C_{3v}$ | 2.308, 2.309 | 1.995 | 1.908 | 1.192 |
| $N_2$–$\{Mo[N_3N]\}_2$ | 0 | $C_1$ | 2.442 | 2.029 | 1.940 | 1.208 |
| | 1 | $C_1$ | 2.437 | 2.031 | 1.944 | 1.208 |
| | | *exptl* | *2.29* | *2.011* | *1.907* | *1.20*[18] |
| N–$Mo[NH_2]_3[NH_3]$ | 0 | $C_{3v}$ | 2.856 | 1.991 | 1.669 | |
| | | $C_1$ | 2.877 | 1.989 | 1.669 | |
| N–$Mo[N_3N]$ | 0 | $C_1$ | 2.477 | 2.035 | 1.681 | |
| | | *exptl* | *2.396* | *2.003* | *1.652*[49] | |

straps. For the full system, however, the QM/MM calculated Mo–$N_{ax}$ bond lengths of 2.380 and 2.477 Å for the reactant and product, respectively, fit within the range of experimental Mo–$N_{ax}$ distances of 2.2 to 2.5 Å.[12,20,21] Consequently, in subsequent model calculations, the Mo–$N_{ax}$ bond was fixed to 2.4 Å for the reactant and product to mimic the constraints of the ligand straps, resulting in an increase in energy of the reactant and product by 10 and 24 kJ mol$^{-1}$, respectively, compared to the fully optimised structures. Apart from the Mo–$N_{ax}$ bond, the model structures with fixed and optimized cap bonds are very similar.

The reactant and product are calculated to have quartet and singlet ground states, respectively, consistent with our earlier calculations on the $Mo[NH_2]_3$ system.[48] However, the quartet/doublet gap in the reactant $Mo[NH_2]_3[NH_3]$ is about 20 kJ mol$^{-1}$ smaller than the calculated value for $Mo[NH_2]_3$ and this decrease should facilitate uptake of $N_2$, as a spin quartet/doublet crossover is required on binding to the reactant. Disregarding the amine cap, the optimised structures of $Mo[NH_2]_3[NH_3]$ and N–$Mo[NH_2]_3[NH_3]$ are similar to those calculated in an earlier study[48] of the three-coordinate analogues $Mo[NH_2]_3$ and N–$Mo[NH_2]_3$ with the amide donors adopting an out-of-plane trigonal disposition around the metal. For both complexes, the $NH_3$ cap is staggered relative to the $MoN_3$ fragment in the lowest energy structures but the orientation of the cap has little effect on the energy of the complex given that staggered and eclipsed conformations differ by only 1 kJ mol$^{-1}$.

The calculated structures for the full ligand system differ from those for the model system in that the amine cap adopts neither an eclipsed or staggered conformation. Instead, the cap is twisted relative to the $MoN_3$ core by approximately 17° for the reactant and 23° for the product. For both the reactant and product, the calculated Mo–$N_{am}$ bond distances for the full ligand system are slightly longer than the values for the model system but in the case of the product, the calculated value is in good agreement with experiment. As expected, the Mo–$N_{ax}$ distances associated with the amine cap are significantly different, between 0.3–0.4 Å shorter than those calculated for the model complexes. Although these values are in much better agreement with experiment, the calculated Mo–$N_{ax}$ distance for the product is still 0.08 Å too long.

The $N_2$–$Mo[NH_2]_3[NH_3]$ encounter complex is calculated to have a doublet ground state, in agreement with previous computational studies,[24] with the quartet lying 100 kJ mol$^{-1}$ higher in energy. Unlike its three-coordinate counterpart $N_2$–$Mo[NH_2]_3$, which has $C_s$ symmetry, owing to the rotation of one ligand by 90°,[48,50,51] the model encounter complex $N_2$–$Mo[NH_2]_3[NH_3]$ retains approximately $C_{3v}$ symmetry. The full ligand $N_2$–$Mo[N_3N]$ structure is very similar to that calculated for the model system and has approximately trigonal $C_3$ geometry. In general, the calculated bond lengths are in good agreement with the reported crystallographic values, although the N–N bond length is overestimated by approximately 0.06 Å. One noticeable difference between the full ligand structures for the reactant and encounter complexes is the 0.17 Å decrease in the Mo–$N_{ax}$ bond in the latter. Clearly, the amine cap interacts more strongly when dinitrogen is coordinated. In both the model and full ligand structures, the N–N bond undergoes slight activation compared to free dinitrogen but in both cases, the bond activation is less than the values calculated for the corresponding three-coordinate system.

The intermediate dimer, for both the model and full ligand systems is calculated to have a triplet ground state and the Mulliken population analysis is consistent with one unpaired electron on each metal centre. The lowest energy $N_2$–$\{Mo[NH_2]_3[NH_3]\}_2$ structure shown in Figure 2 has $C_{3v}$ symmetry. Unlike the $Mo[NH_2]_3$ system, rotation of the $NH_2$ ligands by 90° is not favourable for the $N_2$–$\{Mo[NH_2]_3[NH_3]\}_2$ dimer in either singlet or triplet spin states, presumably due to the steric interactions between the amide ligands and the amine cap.

The spin-singlet and -triplet full ligand structures for the intermediate dimer are similar to those calculated for the model system and possess approximately $S_3$ symmetry. The calculated Mo–$N_{ax}$ bond length of 2.437 Å for the full ligand system is 0.14 Å longer than the experimental value and also 0.23 Å longer than the Mo–$N_{ax}$ bond in the encounter complex, indicating that the metal-amine cap interaction is weaker in the intermediate dimer. This can be attributed to the greater activation of $N_2$ in the intermediate dimer, which in turn strengthens the Mo–$N_2$ bond while weakening Mo–$N_{ax}$ bond as a result of the *trans* effect. Apart from the Mo–$N_{ax}$ bond, all other calculated bond lengths in Table 1

  

for the intermediate dimer are in good agreement with the reported structures. In particular, the calculated N–N bond length of 1.208 Å for the full ligand system is in excellent agreement with experiment. On the basis of the calculated N–N bond length of 1.221 Å for the three-coordinate $N_2$–$\{Mo[NH_2]_3\}_2$ dimer, the N–N bond activation in $N_2$–$\{Mo[N_3N]\}_2$ is weaker, consistent with the crystallographic values.

The energies of the encounter complex, intermediate dimer and product species relative to reactants for both the model $Mo[NH_2]_3[NH_3]$ and full ligand $Mo[N_3N]$ systems are listed in Table 2 and plotted in Figure 3 with the values for the model three-coordinate $Mo[NH_2]_3$ system included for comparison.[48,52] For the model system, the energies of the reactant and product species are reported for both the minimum energy structures and for structures in which the Mo–$N_{ax}$ distance was fixed to 2.4 Å in order to mimic the constraints of the ligand straps. Full DFT single point calculations were also carried out on the QM/MM optimised geometries of the full ligand system.

Table 2. The calculated potential energies and free energies (in italics) in kJ mol$^{-1}$ of encounter complex, intermediate dimer and product relative to reactants for the reaction of $N_2$ with $Mo[NH_2]_3[NH_3]$ and $Mo[N_3N]$ R = *t*Bu. Values for $Mo[NH_2]_3$ are included for comparison.[48,52]

| System | Mo–$N_{ax}$ | $N_2$ complex | Intermediate dimer | | Product |
|---|---|---|---|---|---|
| | | | $S=0$ | $S=1$ | |
| $Mo[NH_2]_3$ | | −71 | −241 | −234 | −335 |
| | | *−24*[a] | *−141* | *−126* | *−275* |
| $Mo[NH_2]_3[NH_3]$ | min | −133 | −347 | −370 | −343 |
| | | *−84* | *−216* | *−253* | *−284* |
| | fixed[b] | −153 | −366 | −389 | −315 |
| | | *−101* | *−250* | *−288* | *−253* |
| $Mo[N_3N]$ QM/MM | | −119 | −245 | −265 | −279 |
| DFT SP[c] | | −127 | −262 | −279 | −323 |

[a] Free energies are given in italics, but are not available for the QM/MM systems. [b] Mo–$N_{ax}$ cap bond fixed at 2.4 Å for reactant and product. [c] Full DFT single point calculations carried out on the QM/MM optimised geometries of the full ligand system.

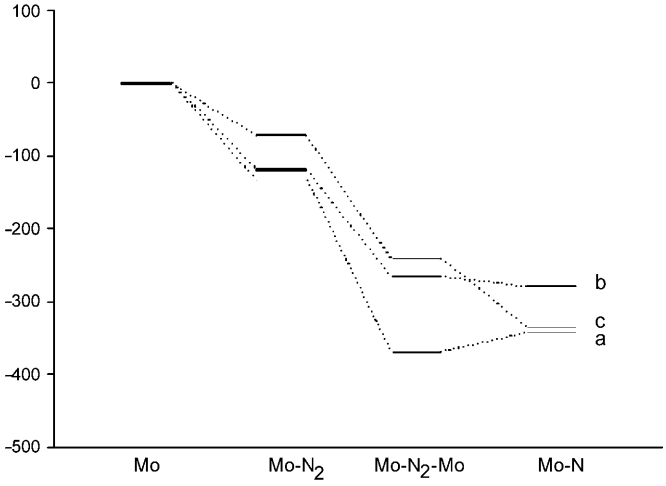


Figure 3. Energies of encounter complex, intermediate dimer and products relative to reactants for a) $Mo[NH_2]_3[NH_3]$, b) $Mo[N_3N]$ and c) $Mo[NH_2]_3$ systems.

The overall reaction of $Mo[NH_2]_3[NH_3]$ with $N_2$ is exothermic with an enthalpy of approximately 343 kJ mol$^{-1}$ for the minimum energy pathway, very close to the calculated value of 335 kJ mol$^{-1}$ for the model three-coordinate $Mo[NH_2]_3$ system. When the Mo–$N_{ax}$ distance is constrained, the exothermicity decreases to 315 kJ mol$^{-1}$ and inclusion of the entropy terms further decreases the stability of the products. Compared to the $Mo[NH_2]_3$ system, the encounter complex and intermediate dimer for both the optimized and constrained $Mo[NH_2]_3[NH_3]$ systems, are more stable relative to the reactants, which may explain why the $N_2$–$Mo[N_3N]$ encounter complex has been isolated in experiment whereas the $N_2$–$Mo[N(R)Ar]_3$ has not. A consequence of this additional stabilisation is that the $N_2$–$\{Mo[NH_2]_3[NH_3]\}_2$ intermediate dimer is much more stable relative to products than for $Mo[NH_2]_3$, making the final N–N cleavage step only favourable by 31 kJ mol$^{-1}$ (free energy) for the minimized structure, and unfavourable by 35 kJ mol$^{-1}$ when the Mo–$N_{ax}$ cap bond is fixed. In contrast, each step of the reaction for the model three-coordinate system is exothermic.

For the full ligand $Mo[N_3N]$ system, the calculated energies of the species along the reaction pathway are less stable relative to reactants than for the model $Mo[NH_2]_3[NH_3]$ system, with an overall reaction exothermicity of 279 kJ mol$^{-1}$. A similar trend was observed for the corresponding three-coordinate $MoL_3$ (L = $NH_2$, N(*t*Bu)Ar) system when the model $NH_2$ ligands were replaced by the bulky N(*t*Bu)Ar groups in the full ligand system.[48,52] The effect of ligand bulk is especially evident for the intermediate dimer which is destabilized by 105 kJ mol$^{-1}$ relative to the optimized model system and even further when the Mo–$N_{ax}$ bond is constrained, bringing it 14 kJ mol$^{-1}$ above the products in energy. The small exothermicity of the N–N cleavage step differs from the calculations of Cui et al[22] for which the same step was calculated to be endothermic by 42 kJ mol$^{-1}$. However, although the model $Mo[N_3N]$ system used by these workers included the ligand straps, it excluded the R groups. Consequently, it makes sense to attribute the additional destabilization of the dimer in the full ligand system to the steric crowding of the R groups between the metal centres. The encounter complex, intermediate dimer and product are all found to be more favourable relative to reactants for the single point full DFT calculations and the overall reaction is calculated to be exothermic by 323 kJ mol$^{-1}$.

The differences in relative energies of the encounter complex and intermediate dimer for the model and full ligand systems raises the question as to whether the reactant and product are destabilised when the amine cap is bound or alternatively, whether the encounter complex and intermediate dimer are stabilised. To address this question, the energy associated with the binding of $NH_3$ to $Mo[NH_2]_3$ along the

  

$C_3$ axis was calculated for each species along the reaction pathway. The calculated energies of reaction are given in Table 3.

Table 3. Estimated energy of reaction for binding of $NH_3$ to $Mo[NH_2]_3$, $N_2$–$Mo[NH_2]_3$, $N_2$–$\{Mo[NH_2]_3\}_2$ and N–$Mo[NH_2]_3$ in $C_{3v}$ symmetry.

| Reaction | Spin | $E$ [kJ mol$^{-1}$] |
|---|---|---|
| $Mo[NH_2]_3+NH_3\rightarrow Mo[NH_2]_3[NH_3]$ | 3/2 | −16 |
| $N_2$–$Mo[NH_2]_3+NH_3\rightarrow N_2$–$Mo[NH_2]_3[NH_3]$ | 1/2 | −74 |
| $N_2$–$\{Mo[NH_2]_3\}_2+2\,NH_3\rightarrow N_2$–$\{Mo[NH_2]_3[NH_3]\}_2$ | 0 | −110 |
| | 1 | −162 |
| N–$Mo[NH_2]_3+NH_3\rightarrow$N–$Mo[NH_2]_3[NH_3]$ | 0 | −16 |

The results show that $NH_3$ only binds weakly to the reactant and product with Mo–$N_{ax}$ bond strengths of 16 kJ mol$^{-1}$ for both, consistent with the relatively long Mo–$N_{ax}$ bond lengths calculated for these two species. If the Mo–$N_{ax}$ bond is shortened to 2.4 Å to reflect the constraints of the ligand straps, the Mo–$N_{ax}$ bond strength is reduced to 7 kJ mol$^{-1}$ in the reactant, whereas in the product the Mo–$N_{ax}$ interaction becomes antibonding by 3 kJ mol$^{-1}$. In contrast, binding of $NH_3$ stabilises the encounter complex by 74 kJ mol$^{-1}$ and the intermediate dimer by 110 kJ mol$^{-1}$ for the singlet spin state and 162 kJ mol$^{-1}$ for the triplet. Because the final N–N bond cleavage step in the three-coordinate $Mo[NH_2]_3$ system is exothermic by 94 kJ mol$^{-1}$, the additional stabilisation of the dimer on binding the amine cap is enough to render this step endothermic for N–$Mo[NH_2]_3[NH_3]$. For the full ligand $Mo[N_3N]$ system, the stabilization of the intermediate dimer due to the metal-cap interaction is offset by the destabilization arising from the ligand bulk, resulting in a slightly exothermic N–N cleavage step.

By itself, the endothermicity of the N–N cleavage step calculated for the model $Mo[NH_2]_3[NH_3]$ system would appear to account for the failure of the experimental system to cleave $N_2$. However, the full ligand calculations reverse this result and so on thermodynamic grounds alone, cleavage of $N_2$ to form the nitride product is predicted for the full ligand $Mo[N_3N]$ system. As this is not observed experimentally, it is necessary to investigate any kinetic barriers present that may prevent $N_2$ cleavage.[20,21] Accordingly, a series of optimizations at varying N–N bond lengths were undertaken for both the model $N_2$–$\{Mo[NH_2]_3[NH_3]\}_2$ and full ligand $N_2$–$\{Mo[N_3N]\}_2$ dimers, the results of which are plotted in Figure 4. The activation barrier for N–N cleavage is estimated at 151 kJ mol$^{-1}$ for the model system which is more than twice the activation barrier calculated for $N_2$ cleavage in the three-coordinate $[H_2N]_3Mo$–$N_2$–$Mo[NH_2]_3$ dimer (66 kJ mol$^{-1}$).[48] Therefore, for the model system, the final N–N cleavage step is not only endothermic but also accompanied by a considerable activation barrier. The estimated activation barrier for $N_2$ cleavage in the full ligand Mo-$[N_3N]$ system is even larger, approximately 213 kJ mol$^{-1}$, and consequently, although the final step is slightly exothermic, N–N cleavage is kinetically unfavourable, consistent with experimental results.

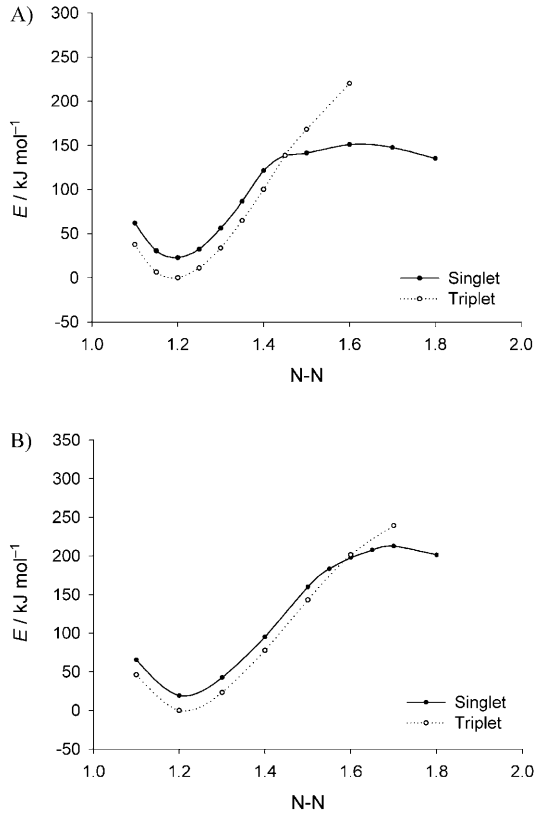


Figure 4. Estimation of the activation barrier to N–N cleavage. Energy versus N–N bond length (Å) for A) the model system; $[H_3N][H_2N]_3Mo$–$N_2$–$Mo[NH_2]_3[NH_3]$ and B) the full ligand system $[N_3N]Mo$–$N_2$–Mo-$[N_3N]$.

**Molecular orbital analysis**: To further probe the effect of the $NH_3$ cap on the bonding in the $Mo[N_3N]$ system, molecular orbital diagrams are shown in Figure 5 for the model reactant $Mo[NH_2]_3[NH_3]$ and product N–$Mo[NH_2]_3[NH_3]$, and in Figure 6 for the intermediate dimer $N_2$–$\{Mo[NH_2]_3$-$[NH_3]\}_2$. These molecular orbital diagrams, which are constructed in $C_{3v}$ symmetry, can be compared with those generated for $Mo[NH_2]_3$, N–$Mo[NH_2]_3$ and $N_2$–$\{Mo[NH_2]_3\}_2$ in an earlier study of the analogous three-coordinate system.[53]

For $Mo[NH_2]_3[NH_3]$, the lone pair of the amine cap interacts with the valence $d_{z^2}$ orbital on Mo. The $d_{xz}$, $d_{yz}$, $d_{xy}$ and $d_{x^2-y^2}$ orbitals on the other hand, are not orientated correctly to interact with the cap, hence the energy of these orbitals are very similar to those calculated for the model $Mo[NH_2]_3$ system. In the reactant, $Mo[NH_2]_3[NH_3]$, the interaction of the cap with the $d_{z^2}$ orbital on Mo forms the $15a_1$ (bonding) and $16a_1$ (antibonding) orbitals shown in Figure 5. The antibonding orbital is primarily the $d_{z^2}$ orbital on Mo (61% Mo $d_{z^2}$, 6% N $p_z$) and therefore binding of the $NH_3$ cap effectively destabilises the $d_{z^2}$ orbital. As a result, the energy gap between the $d_{z^2}$ and $d_{yz}$, $d_{xz}$ orbitals increases from 0.16 to 0.71 eV, leading to a smaller spin doublet/quartet energy gap. The antibonding nature of the Mo $d_{z^2}$ orbital with respect to the $NH_3$ lone pair accounts for the tendency of Mo-$[NH_2]_3[NH_3]$ to repel the amine cap. The presence of the

  

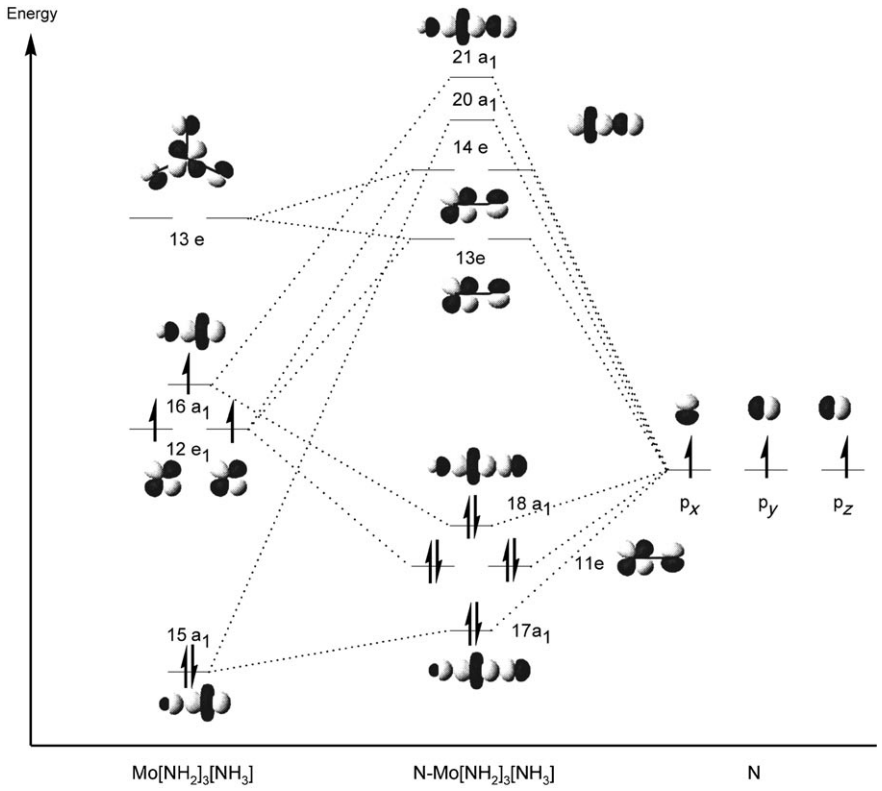


Figure 5. Molecular orbital diagram for N–Mo$[NH_2]_3[NH_3]$ in $C_{3v}$ symmetry. In the N–Mo$[NH_2]_3[NH_3]$ product, the metal $d_{xz}$ and $d_{yz}$ orbitals (12e) undergo π interactions with the $p_x$ and $p_y$ orbitals of the terminal nitrogen atom. The 13e orbital of Mo$[NH_2]_3[NH_3]$ is non-bonding with respect to the metal-nitrogen bond but mixes with the metal-nitrogen π* orbitals, which are close in energy, to form the 13e and 14e orbitals. This interaction also occurs for N–Mo$[NH_2]_3$. The reactant and product energies were adjusted on the basis of the non-bonding $1a_2$ orbital (not shown).

amine cap has a similar impact on the bonding in the product, N–Mo$[NH_2]_3[NH_3]$. In this case however, as the bonding and antibonding $17a_1$ and $18a_1$ levels in Figure 5 are both doubly occupied, the interaction between Mo and the $NH_3$ cap is essentially non-bonding, consistent with the calculated $NH_3$ binding energy in Table 3

The simplified molecular orbital diagram shown in Figure 6 for the optimised geometries of both $N_2$–{Mo$[NH_2]_3[NH_3]$}$_2$ and $N_2$–{Mo$[NH_2]_3$}$_2$, and also for the former with the Mo–$N_{ax}$ cap distance fixed at 4.0 Å, focuses on the valence d orbitals on Mo and the π and π* orbitals of $N_2$. The lone pair on the amine cap interacts with the $30a_1$ and $31a_1$ orbitals of $N_2$–{Mo$[NH_2]_3$}$_2$ in an antibonding manner, raising their energy by over 1.5 eV. As both these orbitals are unoccupied while the lower-lying bonding orbitals (not shown) associated with the Mo–$N_{ax}$ cap interaction are occupied, a net stabilisation of the dimer results. Although not shown, the bonding in $N_2$–Mo$[NH_2]_3[NH_3]$ is similar, and as a result, binding of the $NH_3$ cap also stabilises the encounter complex in the doublet spin state.

Binding of the amine cap and the resulting *trans* effect, leads to an increase in the Mo–$N_2$ bond length. The energy of the 22e orbital in $N_2$–{Mo$[NH_2]_3$}$_2$, which has significant Mo–$N_2$ π bonding character, therefore increases. As this orbital is responsible for the back-bonding from the metal into the π* orbitals on $N_2$, the level of $N_2$ activation in $N_2$–{Mo$[NH_2]_3[NH_3]$}$_2$ compared to $N_2$–{Mo$[NH_2]_3$}$_2$ is expected to decrease. The 0.03 Å reduction in the calculated N–N bond length for $N_2$–{Mo$[NH_2]_3$-$[NH_3]$}$_2$ compared to $N_2$–{Mo-$[NH_2]_3$}$_2$ is consistent with this prediction.

**Bonding analysis**: To quantify energetically the effect of the amine cap on $N_2$ activation, a bonding analysis was undertaken for the Mo–$N_2$ and N–N bonds in the model $[H_3N]$-$[H_2N]_3$Mo–$N_2$–Mo$[NH_2]_3[NH_3]$ intermediate dimer. To analyse the N–N bond, the molecule was separated into two $[H_3N]$-$[H_2N]_3$Mo–N fragments, represented as LMoN–NMoL in Table 4, whereas for the Mo–$N_2$ bonds, the molecule was partitioned into two $[H_3N][H_2N]_3$Mo fragments and one $N_2$ fragment, represented as LMo–$N_2$–MoL. Unfortunately, it is necessary to use the model dimer for this analysis as the lower symmetry of the full ligand Mo$[N_3N]$ system makes it impossible to cleanly partition the bonding energy into σ and π contributions.

The interaction energy between the fragments was determined from a single point calculation, corresponding to the fully optimised geometry of the intermediate dimer. The analysis was repeated with the Mo–$NH_3$ cap bond fixed at 4.0 Å which approximates the bonding in the intermediate dimer when the amine cap is essentially unbound. The bonding energy between the fragments was then broken down into Pauli, electrostatic and orbital contributions, according to Equation (1):

$$E_B = E_{elect} + E_{Pauli} + E_{orb} \quad (1)$$

in which $E_{elect}$ measures the electrostatic interactions between the fragments, $E_{Pauli}$ is the four-electron two-orbital repulsive term, and $E_{orb}$ is the orbital interaction term which can be further partitioned into contributions from each of the irreducible representations of the point group. Because the intermediate dimer has $C_{3v}$ symmetry, the orbital contribution to the bond energy can be decomposed into contributions from the $A_1$, $A_2$ and $E$ irreducible representations. The $A_1$ contribution arises from the σ bonding interaction where-

  

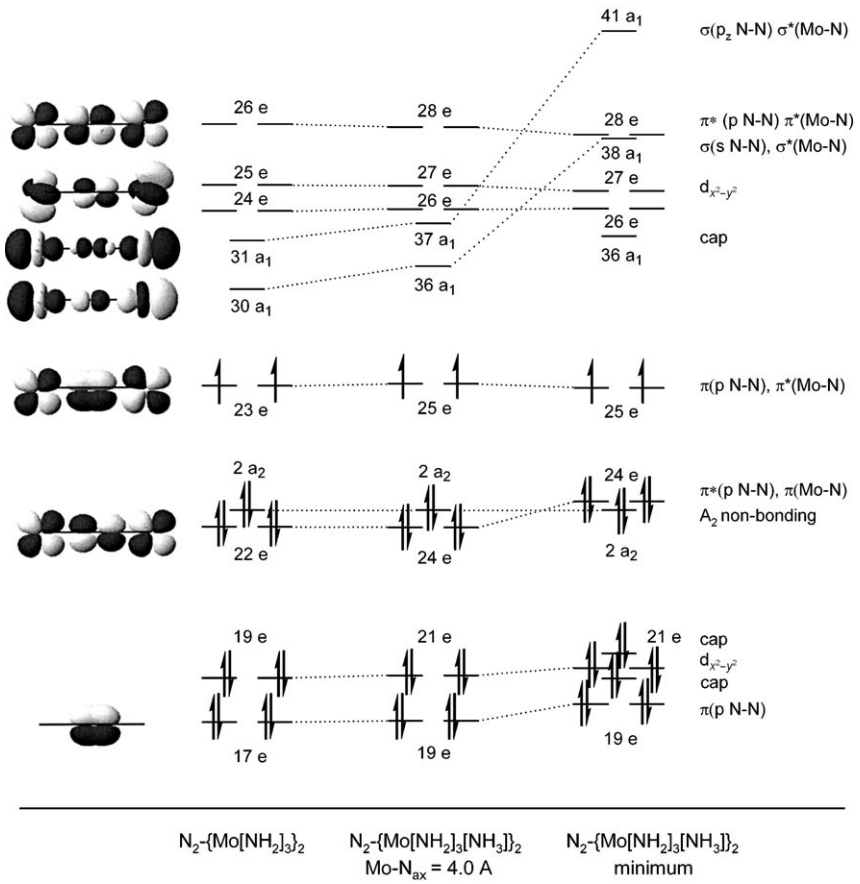


Figure 6. Simplified molecular orbital diagram in $C_{3v}$ symmetry for the optimised structures of $N_2$–$\{Mo[NH_2]_3\}_2$ and $N_2$–$\{Mo[NH_2]_3[NH_3]\}_2$ dimers and also for the latter with the Mo–$N_{ax}$ fixed at 4.0 Å. Energies were adjusted relative to the non-bonding $1a_2$ orbital (not shown).

Overall, the results show a decrease in Mo–$N_2$ bond energy and a slight increase in N–N bond strength on binding the $NH_3$ cap which can be attributed to the *trans* effect. The results are also consistent with the destabilization of the 24e orbital in Figure 6 for $N_2$–$\{Mo[NH_2]_3[NH_3]\}_2$ which is largely Mo–$N_2$ bonding and N–N antibonding. The relative σ/π bonding ratio, electrostatic/orbital ratio and N–N bond strength do not change substantially when the $NH_3$ cap binds. The partitioning of the orbital interaction energy into $A_1(\sigma)$ and $E(\pi)$ symmetry contributions reveals that N–N σ bond interaction in the intermediate dimer is approximately twice the π interaction, and this σ/π ratio is very close to that in free $N_2$. In contrast, the Mo–$N_2$ bonding is dominated by the π interaction, as the $E(\pi)$ contribution is almost three times $A_1(\sigma)$.

In the case of the LMo–$N_2$–MoL fragment bonding analysis, the $E(\pi)$ contribution is the sum of both the π forward- and back-bonding interactions involving the metal and $N_2$ fragment. Thus, in order to distinguish between these two interactions, it is necessary to perform an additional bond decomposition analysis for which the π* orbitals of $N_2$ are removed. The difference in the relative contributions to the bonding energy between this and the previous analysis can then be attributed to backbonding interactions involving the $d_\pi$ orbitals on Mo and the π* orbitals of $N_2$.

The change in the orbital contributions to the bonding energy on removal of the $N_2$ π* orbitals, denoted $\Delta A_1$ and $\Delta E$, are listed in Table 5. The changes in the $A_1$ contribution are relatively small as there are no orbitals of this symmetry involved in backbonding. The $E(\pi)$ contribution, on the other hand, changes by 6.14 eV for the minimum geometry as the $E$ contribution relates to the π bonding. The $A_2$ contribution is negligible as there are no bonding orbitals of this symmetry, consequently, this term is omitted in the following discussion. As the σ and π interactions span different irreducible representations, it is possible to examine σ and π bonding effects between the fragments independently. The results of the bond decomposition analysis are shown in Table 4 along with the relevant values for free $N_2$.

Table 4. Bond energy decomposition for the N–N, LMoN–NMoL and LMo–$N_2$–MoL bonds in the model $N_2$–$\{Mo[NH_2]_3[NH_3]\}_2$ intermediate dimer in $C_{3v}$ symmetry.

| Bond | Mo–$N_{ax}$ | $E_{Pauli}$ [eV] | $E_{elstat}$ [eV] | $E_{orb}$ [eV] $A_1$ (σ) | E (π) | Total | $E_B$ [eV] |
|---|---|---|---|---|---|---|---|
| N–N | | 34.54 | −13.47 | −20.67 | −10.72 | −31.39 | −10.32 |
| LMoN–NMoL | min | 25.85 | −8.98 | −16.51 | −8.98 | −25.49 | −8.62 |
| | fixed[a] | 23.43 | −7.74 | −16.02 | −8.16 | −24.19 | −8.51 |
| LMo–$N_2$–MoL | min | 10.96 | −5.82 | −2.67 | −7.92 | −10.59 | −5.45 |
| | fixed[a] | 12.91 | −6.58 | −3.39 | −9.64 | −13.03 | −6.70 |

[a] Mo–$N_{ax}$ cap bond fixed at 2.4 Å.

Table 5. The change in the orbital contributions to the bonding energy (eV) when the $N_2$ π* orbitals are removed in the model $N_2$–$\{Mo[NH_2]_3[NH_3]\}_2$ intermediate dimer in $C_{3v}$ symmetry.

| Mo–$N_{ax}$ | $\Delta A_1$ (σ) | $\Delta E$ (π) | ΔTotal |
|---|---|---|---|
| min | 0.53 | 6.14 | 6.67 |
| fixed[a] | 0.68 | 7.40 | 8.08 |

[a] Mo–$N_{ax}$ cap bond fixed at 2.4 Å.

  

and 7.40 eV if the Mo–$NH_3$ distance is fixed at 4.0 Å. In both cases, this change represents almost 80% of the total $E(\pi)$ contribution, indicating that π back-bonding forms the major part of the metal-$N_2$ π interaction. As $\Delta E(\pi)$ is reduced by nearly 1.3 eV when the $NH_3$ cap is bound, one can conclude that binding of the amine cap reduces back-donation from the metal into the $N_2$ π* orbitals. This is contrary to the expectations of O'Donoghue et al who suggested that coordination of the apical nitrogen may promote more efficient back-bonding.[21]

On the basis of the above bond decomposition analysis and the calculation of the overall reaction profile presented earlier, the inability of $Mo[NH_2]_3[NH_3]$ to cleave $N_2$ is owed to a combination of factors including the increased stability of the $N_2$–$\{Mo[NH_2]_3[NH_3]\}_2$ dimer upon binding the amine cap, the reduction in N–N activation as a result of less efficient back-donation from the metal into the $N_2$ π* orbitals, and the relatively high kinetic barrier to cleavage. Although the situation will be slightly different in the full ligand Mo[$N_3$N] system in which steric crowding also plays an important role, the effect of the ligand cap on the binding and activation of $N_2$ should be similar.

## Conclusion

The reaction of $N_2$ with the model $Mo[NH_2]_3[NH_3]$ and full ligand Mo[$N_3$N] systems was explored using density functional theory. Structurally, the calculations reveal that the amine cap is bound in both the encounter complex and intermediate dimer but essentially unbound in the reactant and product species, giving rise to long Mo–$N_{ax}$ bond distances in excess of 2.60 Å for the model system and up to 2.48 Å in the full ligand system in which the lengthening of the Mo–$N_{ax}$ cap bond is limited by the ligand straps.

The overall reaction is calculated to be exothermic for both systems, but although the final N–N cleavage step is endothermic by 75 kJ mol$^{-1}$ for the model system when the Mo–$N_{ax}$ bond length is fixed to model the constraints of the ligand straps, it is slightly exothermic by 14 kJ mol$^{-1}$ for the full ligand system. In general, the species along the reaction pathway are not as stable relative to the reactants for the full ligand system, which can be attributed to the presence of the bulky R group substituents and the ligand straps. This difference in energetics is particularly evident for the intermediate dimer in which the steric crowding between the metal centres is more significant.

The activation barrier for N–N cleavage is estimated at 151 kJ mol$^{-1}$ for the model system, more than twice the activation barrier calculated for N–N cleavage in the model three-coordinate $[H_2N]_3Mo$–$N_2$–$Mo[NH_2]_3$ dimer, and approximately 213 kJ mol$^{-1}$ for the full ligand [$N_3$N]Mo–$N_2$–Mo[$N_3$N] system. Therefore, although the final step is slightly exothermic for the full ligand system, N–N cleavage is kinetically unfavourable, accounting for why the reaction does not proceed beyond the [$N_3$N]Mo–$N_2$–Mo[$N_3$N] dimer in experiment.

A MO analysis showed that the tendency for both the reactant and product species to repel the amine cap is due to the occupation of the antibonding orbital arising from the interaction of the lone pair on the amine cap with the Mo $d_{z^2}$ orbital. In contrast, this orbital is not occupied in both the encounter complex and intermediate dimer leading to binding of the amine cap and much shorter Mo–$N_{ax}$ distances. The binding of the amine cap stabilises both the encounter complex and intermediate dimer, and in the case of the model system, results in an endothermic $N_2$ cleavage step. For the full ligand system, the additional stabilization is offset by the effects of steric crowding in the intermediate dimer and so the final cleavage step remains slightly exothermic.

A bond decomposition analysis of the N–N and Mo–$N_2$ bonds in the $[N_3N]_3Mo$–$N_2$–Mo[$N_3$N] dimer showed that the Mo–N bond strength decreased whereas the N–N bond strength increased slightly as a result of the *trans* effect on binding the amine cap. Binding of the amine cap was also shown to reduce backdonation from the metal into the $N_2$ π* orbitals by nearly 1.3 eV, accounting for the much higher kinetic barrier to cleavage and longer N–N bond distance in the intermediate dimer compared to its three coordinate $Mo[NH_2]_3$ counterpart. Therefore, the inability of Mo[$N_3$N] to cleave $N_2$ can be attributed to the combined effects of the increased stability of the $N_2$–$\{Mo[N_3N]\}_2$ dimer upon binding the ligand cap, less efficient backdonation from the metal into the $N_2$ π* orbitals, and the relatively large kinetic barrier to N–N bond cleavage.

The results of this study suggest that it may be possible to design a related system which is capable of $N_2$ cleavage. One option is to replace the amine cap with a group which does not have a strong interaction with the metal, for example the CMe cap in the $H_3C$-$C(CH_2NHR)_3$ ligand (R = $CH_3$, $C_2H_5$ or $CH(CH_3)_2$).[54] This ligand system has been used to synthesise the $N_2$–$\{V[(i\text{PrHNCH}_2)_3\text{CMe}]\}_2$ dimer with $N_2$ bridging the metal centres[55] but no N–N cleavage was reported. Based on our earlier study of the metal dependence of $N_2$ activation in $M[N(R)Ar]_3$ complexes,[48] we predict that N–N cleavage should be favourable in the $N_2$–$\{M[(i\text{PrHNCH}_2)_3\text{CMe}]\}_2$ system if $V^{III}$ is replaced by a $d^3$ metal from the 2nd or 3rd transition series such as $Mo^{III}$.

## Acknowledgements

The authors gratefully acknowledge the Australian Research Council for financial support in the form of an Australian Postgraduate Award for GC and a Discovery Project Grant for RS and BFY. The Australian National University is also acknowledged for access to the APAC (Australian Partnership for Advanced Computing) supercomputing facilities.

[1] F. Tuczek, N. Lehnert, *Angew. Chem.* **1998**, *110*, 2780–2782; *Angew. Chem. Int. Ed.* **1998**, *37*, 2636–2638.
[2] M. D. Fryzuk, S. A. Johnson, *Coord. Chem. Rev.* **2000**, 200–202, 379–409.
[3] M. P. Shaver, M. D. Fryzuk, *Adv. Synth. Catal.* **2003**, *345*, 1061–1076.
[4] B. A. MacKay, M. D. Fryzuk, *Chem. Rev.* **2004**, *104*, 385–401.

  

[5] M. D. Fryzuk, *Chem. Rec.* **2003**, *3*, 2–11.
[6] C. C. Cummins, *Chem. Commun.* **1998**, 1777–1786.
[7] D. V. Yandulov, R. R. Schrock, *Science* **2003**, *301*, 76–78.
[8] D. V. Yandulov, R. R. Schrock, *J. Am. Chem. Soc.* **2002**, *124*, 6252–6253.
[9] G. J. Leigh, *Science* **2003**, *301*, 55–56.
[10] R. R. Schrock, *Acc. Chem. Res.* **1997**, *30*, 9–16.
[11] K. Y. Shih, K. Totland, S. W. Seidel, R. R. Schrock, *J. Am. Chem. Soc.* **1994**, *116*, 12103–12104.
[12] N. C. Mösch-Zanetti, R. R. Schrock, W. M. Davis, K. Wanninger, S. W. Seidel, M. B. Odonoghue, *J. Am. Chem. Soc.* **1997**, *119*, 11037–11048.
[13] N. C. Zanetti, R. R. Schrock, W. M. Davis, *Angew. Chem.* **1995**, *107*, 2148–2186; *Angew. Chem. Int. Ed.* **1995**, *34*, 2044–2046.
[14] M. J. Byrnes, X. L. Dai, R. R. Schrock, A. S. Hock, P. Muller, *Organometallics* **2005**, *24*, 4437–4450.
[15] C. E. Laplaza, C. C. Cummins, *Science* **1995**, *268*, 861–863.
[16] C. E. Laplaza, A. L. Odom, W. M. Davis, C. C. Cummins, J. D. Protasiewicz, *J. Am. Chem. Soc.* **1995**, *117*, 4999–5000.
[17] C. E. Laplaza, M. J. A. Johnson, J. C. Peters, A. L. Odom, E. Kim, C. C. Cummins, G. N. George, I. J. Pickering, *J. Am. Chem. Soc.* **1996**, *118*, 8623–8638.
[18] K. Y. Shih, R. R. Schrock, R. Kempe, *J. Am. Chem. Soc.* **1994**, *116*, 8804–8805.
[19] J. J. Curley, T. R. Cook, S. Y. Reece, P. Müller, C. C. Cummins, *J. Am. Chem. Soc.* **2008**, *130*, 9394–9405.
[20] M. Kol, R. R. Schrock, R. Kempe, W. M. Davis, *J. Am. Chem. Soc.* **1994**, *116*,4382–4390.
[21] M. B. O'Donoghue, W. M. Davis, R. R. Schrock, *Inorg. Chem.* **1998**, *37*, 149–5158.
[22] Q. Cui, D. G. Musaev, M. Svensson, S. Sieber, K. Morokuma, *J. Am. Chem. Soc.* **1995**, *117*, 12366–12367.
[23] M. B. O'Donoghue, N. C. Zanetti, W. M. Davis, R. R. Schrock, *J. Am. Chem. Soc.* **1997**, *119*, 2753–2754.
[24] F. Studt, F. Tuczek, *Angew. Chem.* **2005**, *117*, 5783–5787; *Angew. Chem. Int. Ed.* **2005**, *44*, 5639–5642.
[25] F. Studt, F. Tuczek, *J. Comput. Chem.* **2006**, 27, 1278–1291.
[26] Z. Cao, Z. Zhou, H. Wan, Q. Zhang, *Int. J. Quantum Chem.* **2005**, 103, 344–353.
[27] B. Le Guennic, B. Kirchner, M. Reiher, *Chem. Eur. J.* **2005**, *11*, (24), 7448–7460.
[28] M. Reiher, B. Le Guennic, B. Kirchner, *Inorg. Chem.* **2005**, *44*, (26), 9640–9642.
[29] G. te Velde, F. M. Bickelhaupt, E. J. Baerends, C. Fonseca Guerra, S. J. A. Van Gisbergen, J. G. Snijders, T. Ziegler, *J. Comput. Chem.* **2001**, *22*, (9), 931–967.
[30] C. Fonseca Guerra, J. G. Snijders, Te Velde, G.; E. J. Baerends, *Theor. Chem. Acc.* **1998**, 99, (6), 391–403.
[31] *Amsterdam Density Functional (ADF)* software, Scientific Computing and Modelling, Vrije University, Amsterdam, The Netherlands, **2002**.
[32] S. H. Vosko, L. Wilk, M. Nusair, *Can. J. Phys.* **1980**, *58*, 1200–1211.
[33] A. D. Becke, *Phys. Rev. A* **1988**, 38, 3098–3100.
[34] J. P. Perdew, *Phys. Rev. B* **1986**, 33, 8822–8824.
[35] G. T. Velde, E. J. Baerends, *J. Comput. Phys.* **1992**, 99, 84–98.
[36] L. Versluis, T. Ziegler, *J. Chem. Phys.* **1988**, *88*, 322–328.
[37] E. van Lenthe, E. J. Baerends, J. G. Snijders, *J. Chem. Phys.* **1993**, *99*, 4597–4610.
[38] E. van Lenthe, E. J. Baerends, J. G. Snijders, *J. Chem. Phys.* **1994**, *101*, 9783–9792.
[39] E. van Lenthe, A. Ehlers, E. J. Baerends, *J. Chem. Phys.* **1999**, *110*, 8943–8953.
[40] L. Y. Fan, T. Ziegler, *J. Phys. Chem.* **1992**, *96*, 6937–6941.
[41] L. Y. Fan, T. Ziegler, *J. Chem. Phys.* **1992**, *96*, 9005–9012.
[42] F. M. Bickelhaupt, E. J. Baerends in Kohn-Sham *Density Functional Theory: Predicting and Understanding Chemistry. In Reviews in Computational Chemistry*, (Eds.: K. B. Lipkowitz, D. B. Boyd), Wiley-VCH, Weinheim, **2000**, Vol. 15, pp. 1–86.
[43] T. Ziegler, A. Rauk, *Inorg. Chem.* **1979**, *18*, 1558–1565.
[44] T. Ziegler, A. Rauk, *Inorg. Chem.* **1979**, *18*, 1755–1759.
[45] T. K. Woo, L. Cavallo, T. Ziegler, *Theor. Chem. Acc.* **1998**, *100*, 307–313.
[46] M. Clark, R. D. Cramer, N. Vanopdenbosch, *J. Comput. Chem.* **1989**, *10*, 982–1012.
[47] A. K. Rappe, C. J. Casewit, K. S. Colwell, W. A. Goddard, W. M. Skiff, *J. Am. Chem. Soc.* **1992**, *114*, 10024–10035.
[48] G. Christian, J. Driver, R. Stranger, *Faraday Discuss.* **2003**, 124, 331–341.
[49] D. V. Yandulov, R. R. Schrock, A. L. Rheingold, C. Ceccarelli, W. M. Davis, *Inorg. Chem.* **2003**, *42*, 796–813.
[50] G. Christian, R. Stranger, *Dalton Trans.* **2004**, *16*, 2492–2495.
[51] G. Christian, R. Stranger, B. F. Yates, D. C. Graham, *Dalton Trans.* **2005**, *5*, 962–968.
[52] G. Christian, R. Stranger, B. F. Yates, C. C. Cummins, *Eur. J. Inorg. Chem.* **2007**.
[53] G. Christian, R. Stranger, B. F. Yates, *Inorg. Chem.* **2006**, *45*, 6851–6859.
[54] L. H. Gade, N. Mahr, *J. Chem. Soc.-Dalton Trans.* **1993**, *4*, 489–494.
[55] N. Desmangles, H. Jenkins, K. B. Ruppa, S. Gambarotta, *Inorg. Chim. Acta* **1996**, *250*, 1–4.

Received: June 10, 2008
Published online: December 3, 2008

  